Erschienen in: Twentyfirst European Photovoltaic Solar Energy Conference : Proceedings of the International Conference / Poortmans, Jozef et al. (Hrsg.). - Munich : WIP-Renewable Energies, 2006. - S. 684-687. - ISBN 978-1-60423-787-0

HYDROGEN PASSIVATION OF EXTENDED DEFECTS IN MULTICRYSTALLINE SILICON SOLAR CELLS

M. Rinio[1], M. Kaes[2], G. Hahn[2], D. Borchert[1]
[1] Fraunhofer Institute for Solar Energy Systems, Laboratory and Service Centre, Auf der Reihe 2, 45884 Gelsenkirchen, Germany, Phone: +49-(0)209-15539-12, Fax: +49-(0)209-1209093, E-mail: markus.rinio@ise.fraunhofer.de
[2] University of Konstanz, Department of Physics, 78457 Konstanz, Germany

ABSTRACT: Two methods of hydrogen bulk passivation in multicrystalline ingot silicon solar cells were compared. After $POCl_3$-emitter diffusion, four different solar cell types were made out of neighbouring wafers. The first wafer was not hydrogen passivated. The second wafer was passivated by firing of hydrogenated silicon nitride (SiN:H). On the third wafer, a microwave induced remote hydrogen plasma (MIRHP) was applied. The fourth wafer was passivated by both techniques. On all wafers, the recombination activity of dislocations was measured by the correlation of light beam induced current (LBIC) with dislocation density topography. Recombination at grain boundaries was examined using LBIC line scans. The spatial resolution of the measurements was 12.5 µm.
Keywords: Multi-Crystalline, Passivation, Recombination, LBIC, Hydrogen

1 INTRODUCTION

Hydrogen passivation by firing of hydrogenated silicon nitride (SiN:H) is well established in industrial production of multicrystalline silicon solar cells. However, the passivation mechanisms are not fully understood. Recently the effect of SiN:H firing and microwave induced remote hydrogen plasma (MIRHP) passivation was compared on ribbon wafers (edge defined film-fed growth (EFG) and string ribbon (SR)) [1, 2]. Topograms of the minority carrier lifetime indicated that MIRHP and SiN:H firing passivate different areas of the wafers. In this recent work, the wafers were investigated using microwave photoconductance decay (µ-PCD) topography with a spatial resolution of only 500 µm. Additionally, the surface passivation with iodine ethanol, that was used, is maybe not completely homogeneous on the wafer surface.

As a first step of our present work, these investigations were applied to neighbouring wafers from a multicrystalline silicon ingot.

To be independent of the iodine ethanol surface treatment and to get a better spatial resolution, we applied the combination of high resolution LBIC topography with microscopic defect analysis [3, 4, 5] to solar cells that were made with different techniques of hydrogen passivation. Single dislocation clusters and grain boundaries, that are penetrating all neighbouring samples, were investigated with respect to their recombination activities.

SiN:H firing takes place at high temperatures above 700 °C, whereas MIRHP is normally applied at about 350 °C. The interesting question for this work is: Are some defects better passivated by SiN:H firing and others better passivated by MIRHP? For this, it is worthy to distinguish between the extended defects with a higher spatial resolution.

2 EXPERIMENT

2.1. Lifetime topography

First, five wafers were damage etched with a CP6 solution. The wafers 2,3,4, and 5 were then phosphorus diffused ($POCl_3$) to produce a double sided 45-50 Ω/□ emitter. Then they were exposed to different hydrogen passivation techniques. The wafers 1 and 2 were not passivated. The third and the fifth wafer were covered with a SiN:H layer of about 75 nm thickness on one side by PECVD and fired at a peak temperature of about 800 °C. The peak duration, where the temperature was above 700 °C, was below 10 s [6]. Afterwards, the SiN and emitter layers were removed on all wafers by etching. The fourth and fifth wafer were then treated with a MIRHP passivation at 350 °C for one hour. Finally, all wafers were etched again in CP6 solution to remove a layer of about 12 µm from both sides and surface passivated in iodine ethanol solution. Topograms of the effective minority carrier lifetime were measured on pieces of 5 cm x 5 cm size by the µ-PCD technique with a spatial resolution of 500 µm.

2.2 LBIC topography and defect analysis

In the main experiment, four neighbouring wafers with a size of 10 cm x 10 cm were cut out of a multicrystalline silicon ingot close to the position of the wafers of our first experiment. Then, four different solar cell processes were applied as indicated in fig. 1. The screen printed Al contact was applied to compensate the rear emitter and to produce a back surface field, which improves the sensivity of the LBIC-measurements to the bulk recombination. Secondly, it protects the bulk from metal contaminations from the firing furnace belt. For the MIRHP treatment, the SiN:H and Al was removed to get a hydrogen diffusion from both sides. At the end, all cells were equipped with equal evaporated contacts using Ti/Pd/Ag on the front side and Al on the rear side. This

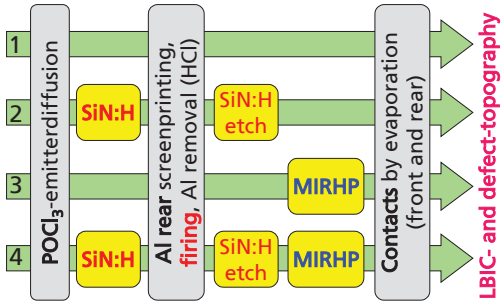

Fig. 1 Schematic solar cell processes that were applied to four neighbouring wafers for the main experiment.

provides a maximum comparability of the cells with respect to the rear surface recombination velocity.

After processing, some hundred LBIC topograms were measured on the solar cells using a single wavelength of 830 nm, a spatial resolution of 12.5 µm, and a light power of 1.7 µW. This system was recently installed at Fraunhofer ISE in Gelsenkirchen. The maps showed the same defect structures on all four neighbouring wafers, which means that the influence of the different hydrogen passivation techniques on the same grain boundaries or dislocation clusters could be studied.

Subsequently, the wafers were cut into smaller pieces, that were polished and exposed to a Secco etch [7] of 60 s duration, which revealed crystal defects like grain boundaries and dislocations. Some thousand microscopic images with a size of about 100 x 150 µm were taken on the etched surfaces. Grain boundaries and artifacts were removed from these pictures manually with a specialised image processing software. The positions of the dislocation etch pits were measured by an image recognition system. Topograms of the dislocation density were calculated from these positions, as described earlier [3].

Pairs of the *IQE* and the dislocation density ρ were collected from all positions within small areas of some 100 µm in diameter. In theory the influence of the dislocation density on the minority carrier diffusion length L is described by Donolato's model for a given normalized recombination strength Γ of the dislocations and a background diffusion length L_0 far away from dislocations and grain boundaries. Γ is the number of recombinations per unit time, length, and excess carrier density, divided by the minority carrier diffusion coefficient D. We combined Donolato's model with a simulation of the function $IQE(L)$ by the computer programme PC1D [8]. The PC1D-simulation contains all special features of the solar cell structure (e. g. thickness, rear surface recombination velocity, emitter profile). We obtained Γ by fitting the theoretical model $IQE(\rho)$ to the experimental data with Γ and L_0 as fit parameters. The detection limit for Γ in our samples is somewhere about 0.0001.

3 RESULTS AND DISCUSSION

3.1. Lifetime topography

Fig. 2 shows the minority carrier lifetime maps of the samples of the first experiment. The topograms reveal, that during emitter diffusion the recombination centres are spatially redistributed. In areas with low densities of extended defects the lifetime is improved by external phosphorus gettering. On the contrary a deterioration of the lifetime is observed in areas with high densities of extended defects. These areas can be recognised by low initial lifetimes. This can be explained by impurities that are internally gettered to grain boundaries and dislocations during emitter diffusion, which leads to a decrease in the lifetime. The results are in good agreement with previous investigations [5].

Both kinds of hydrogen passivation mainly improve the regions with low lifetimes (high defect densities). However, the maps show also differences between MIRHP and SiN:H firing. In area A, lower lifetimes were measured after SiN:H firing than after MIRHP. The opposite result is found in area B. Because the measured lifetimes in area A and B are between 80 and 300 µs, this has no considerable effect on solar cells. For 80 µs, the diffusion length is already 470 µm, which is much larger than the cell thickness of 270 µm. Additionally, it is possible, that the different behaviour in areas A and B is due to an inhomogeneous surface passivation by the iodine ethanol passivation at the wafer edges. All in all, the SiN:H firing seems to produce a slightly better passivation than MIRHP.

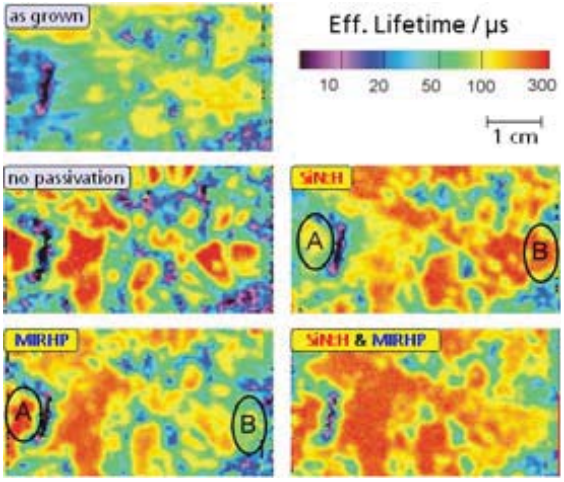

Fig. 2 Effective minority carrier lifetime measured by the µ-PCD-method using an iodine ethanol surface passivation. The five maps were measured on neighbouring wafers, that were treated with different hydrogen passivation techniques. The first map (upper image) shows the as-grown wafer. The next four maps were measured on the phosphorus diffused wafers. The method of hydrogen passivation is marked on each map.

3.2. LBIC topography and defect analysis

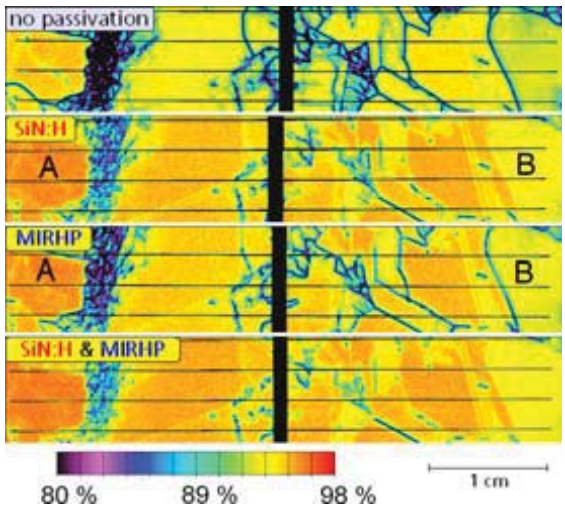

Fig. 3 *IQE* maps of the four solar cells measured by LBIC at a wavelength of 830 nm with a spatial resolution of 50 µm. The marked positions A and B correspond to the areas A and B in fig. 2 (neighbouring wafers). On all positions (including A and B), SiN:H firing led to higher *IQE*-values than MIRHP.

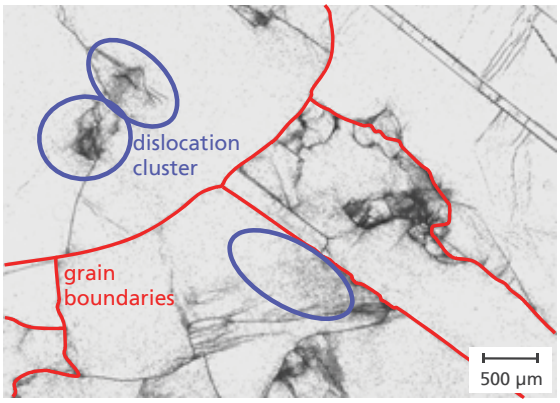

Fig. 4 Microscopic image on the unpassivated solar cell after Secco-etching. Some grain boundaries are marked red and some dislocation clusters, where *IQE*(ρ)-curves were measured, are marked blue.

Fig. 3 shows *IQE* map sections of all four wafers that were processed into solar cells as described in fig. 1. On these maps as well as on more than hundred other maps measured on the four solar cells, the SiN:H firing resulted in better passivation than the MIRHP treatment within all areas. The best passivation was obtained by a combination of both techniques (SiN:H firing and MIRHP).

Fig. 4 exhibits a small section of the unpassivated solar cell after polishing and Secco-etching. The corresponding LBIC maps on all neighbouring wafers is shown in fig. 5. Large fractions of this section contain noticeable densities of dislocations. We also find some grain boundaries within the section. These extended defects show a strong influence on the *IQE*, if no bulk passivation was applied. The LBIC maps reveal, that SiN:H firing leads to a better passivation than MIRHP for all defects within the section. The best passivation was obtained by the combination of SiN:H firing and MIRHP.

On all wafers, several dislocation clusters were analysed by fitting Donolato's theory to the experimental *IQE*(ρ) curves. Fig. 7 shows the results obtained for the marked dislocation cluster in the lower middle of fig. 4. The corresponding Γ values are presented as cluster D together with other clusters in fig. 8.

After hydrogen passivation, the recombination strengths Γ of the dislocations were near to the detection limit of approx. 0.0001. Nevertheless, it was possible to extract the Γ-values shown in fig. 8. In all cases, the SiN:H firing was superior to MIRHP, except for cluster C, where the statistical error was probably greater than the difference between the Γ-values.

In average, the recombination strength of the dislocations was reduced to 9 % of its initial value (no passivation) by SiN:H firing, 13 % by MIRHP, and 4 % by SiN:H firing & MIRHP. For the investigated dislocation clusters, with the combination of SiN:H firing and MIRHP, a double dislocation density had a comparable effect as if only SiN:H firing would have been applied.

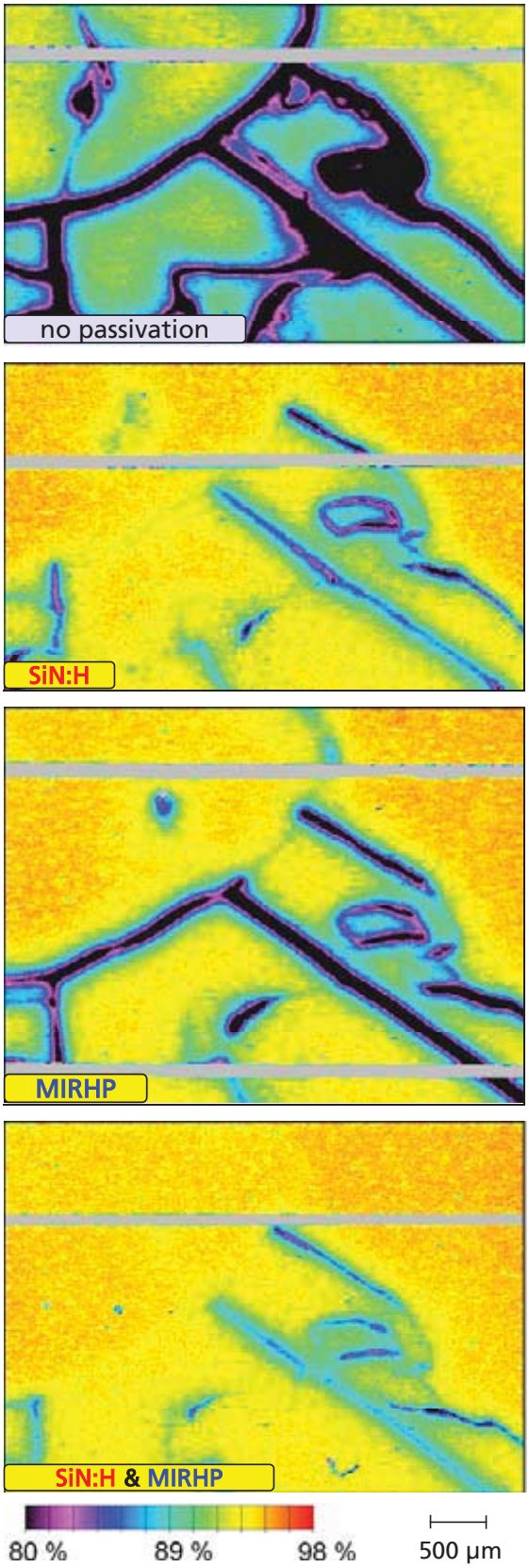

Fig. 5 *IQE* maps on the four solar cells, measured at 830 nm. All maps show the same section as fig. 4. The horizontal grey lines correspond to contact fingers.

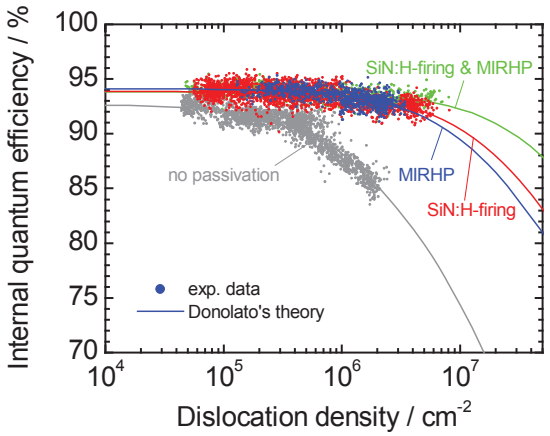

Fig. 7 Correlation of the *IQE* with the dislocation density within the dislocation cluster, which is marked blue in the lower middle of fig. 4. Every measured point belongs to one position within the cluster. The lines shows the result of a fit of Donolato's theory to the measured points. Each solar cell is shown in a different colour.

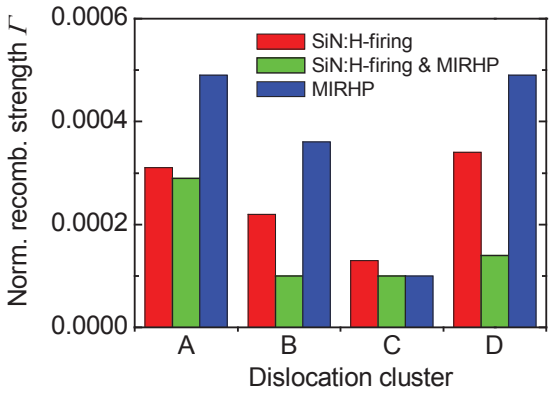

Fig. 8 Γ-values of different dislocation clusters, measured by fitting Donolato's theory to the experimental data. The detection limit for Γ is about 0.0001. The fitting was done completely automatically.

A very similar behaviour is observed at grain boundaries. An example is given in fig. 6, which shows the LBIC linescans perpendicular to a random grain boundary. The recombination activity of this special grain boundary is only weakly reduced by MIRHP. A strong passivation is observed after SiN:H firing. The best passivation is obtained with the combination of SiN:H firing and MIRHP. As can be seen in fig. 5, there exist also grain boundaries, that are almost invisible after a sole MIRHP treatment.

4 CONCLUSION

From these first results, it seems to be likely, that firing of SiN:H layers is superior to MIRHP. No strong evidence was found, that some types of defects are better passivated at 350 °C by MIRHP while others are better passivated at above 700 °C by SiN:H firing.

Best results were achieved with a combination of both hydrogen passivation techniques.

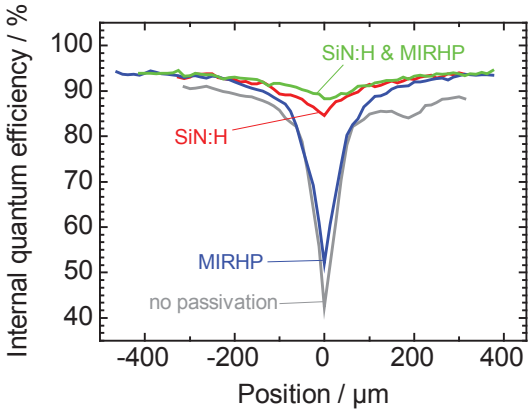

Fig. 6 LBIC-linescans over the same random grain boundary measured with 830 nm wavelength on the four solar cells

ACKNOWLEDGEMENTS

The authors would like to thank S. Riepe for his support with the image recognition system, G. Räuber for polishing of the samples, K. Schmidt and M. Rossow for their contributions to the solar cell processes and O. Al-Kabbani for reviewing all the LBIC maps.

REFERENCES

[1] M. Kaes, G. Hahn, A. Metz, Proc. 31st IEEE PVSC, Lake Buena Vista (2005), p. 923

[2] M. Kaes, G. Hahn, T. Pernau, A. Metz, Proc. 20th EC PVSEC, Barcelona (2005), p. 1063

[3] M. Rinio, S. Peters, M. Werner, A. Lawerenz, H. J. Möller, Solid State Phenomena, **82–84**, (Diffusion and Defect Data / B) (2002), p. 701

[4] M. Rinio, A. Hauser, H. J. Möller, 3rd WCPEC, Osaka, Arisumi Printing Inc, Vol.1 (2003), p. 118

[5] M. Rinio, E. Zippel, D. Borchert, Proc. 20th EC PVSEC, Barcelona (2005), p. 706

[6] F. Huster, Proc. 20th EC PVSEC, Barcelona (2005), p. 1466

[7] F. Secco d'Aragona, J. Electrochem. Soc., **119** (7) (1972), p. 948

[8] P. Basore, D. A. Clugston, 25th IEEE PVSC (1996), p. 377